Received: 12 May 2019 | Revised: 26 November 2019 | Accepted: 28 November 2019

DOI: 10.1002/jbm.a.36861

ORIGINAL ARTICLE

Electrospinning of tyrosine-based oligopeptides: Self-assembly or forced assembly?

Yasaman Hamedani[1,2] | Prathyushakrishna Macha[1,2] | Elvira L. Evangelista[1,2] | Vamshikrishna R. Sammeta[3] | Vijaya Chalivendra[4] | Sivappa Rasapalli[3] | Milana C. Vasudev[1]

[1]Department of Bioengineering, University of Massachusetts Dartmouth, Dartmouth, Massachusetts

[2]Biomedical Engineering and Biotechnology Program, University of Massachusetts Dartmouth, Dartmouth, Massachusetts

[3]Department of Chemistry and Biochemistry, University of Massachusetts Dartmouth, Dartmouth, Massachusetts

[4]Department of Mechanical Engineering, University of Massachusetts Dartmouth, Dartmouth, Massachusetts

Correspondence
Milana C. Vasudev, Department of Bioengineering, University of Massachusetts Dartmouth, Dartmouth, MA 02747.
Email: mvasudev@umassd.edu

Funding information
University of Massachusetts Dartmouth Provost's office; National Science Foundation, Grant/Award Number: 1726239

Abstract

Short oligomeric peptides typically do not exhibit the entanglements required for the formation of nanofibers via electrospinning. In this study, the synthesis of nanofibers composed of tyrosine-based dipeptides via electrospinning, has been demonstrated. The morphology, mechanical stiffness, biocompatibility, and stability under physiological conditions of such biodegradable nanofibers were characterized. The electrospun peptide nanofibers have diameters less than 100 nm and high mechanical stiffness. Raman and infrared signatures of the peptide nanofibers indicate that the electrostatic forces and solvents used in the electrospinning process lead to secondary structures different from self-assembled nanostructures composed of similar peptides. Crosslinking of the dipeptide nanofibers using 1,6-diisohexanecyanate (HMDI) improved the physiological stability, and initial biocompatibility testing with human and rat neural cell lines indicate no cytotoxicity. Such electrospun peptides open up a realm of biomaterials design with specific biochemical compositions for potential biomedical applications such as tissue repair, drug delivery, and coatings for implants.

KEYWORDS
crosslinking, electrospinning, nanofibers, neural cells, peptides

1 | INTRODUCTION

Peptide-based materials are attractive for biomedical applications such as tissue repair and drug delivery due to their tailorable biochemical and physical properties (Habibi, Kamaly, Memic, & Shafiee, 2016; Zhang, Fei, Yan, Wang, & Li, 2015). Self-assembly of peptide nanostructures is promoted by a solvent-switching process or through methods such as vapor deposition (Adler-Abramovich et al., 2009; Vasudev et al., 2014). Electrospinning is another technique which is a versatile and non-mechanical method wherein the application of electrostatic force leads to the formation of continuous micro/nanoscale nanofibers from a polymeric solution. Biocompatibility and biodegradability are crucial for nanofibers used as biomaterials due to direct or indirect contact with the human body (Holzapfel et al., 2013; Wu, 2014). Electrospun fibrous scaffolds are attractive due to their high surface area and porosity, which mimic the characteristic features of extracellular matrix and have shown enhanced interactions with cells in tissue engineering applications (Grafahrend et al., 2010). Modified electrospinning techniques have also been used for the deposition of aligned nanofibers for directed cell growth, and coaxial electrospinning has been successfully used for drug delivery applications (Kai, Liow, & Loh, 2014; Koh, Yong, Chan, & Ramakrishna, 2008).

In the recent years, there has been considerable interest in the electrospinning of proteins and short peptides for biomedical applications owing to their biocompatibility, but most of these utilize polymers blended with the proteins to enhance mechanical properties, thermal stability and degradability (Khadka & Haynie, 2012; Mendes, Stephansen, & Chronakis, 2017).

Yasaman Hamedani and Prathyushakrishna Macha contributed equally.

Successful examples of electrospun biological molecules have utilized relatively large proteins such as silk, chitin, and collagen (Elsabee, Naguib, & Morsi, 2012; Min et al., 2004; Rho et al., 2006). However, studies involving electrospinning of oligomeric and dimeric peptides are sparse and have yet to be successful in the synthesis of uniform and continuous fibers (Nuansing et al., 2013; Singh, Bittner, Loscher, Malinowski, & Kern, 2008; Tayi, Pashuck, Newcomb, McClendon, & Stupp, 2014). The ability to synthesize nanofibers composed of oligopeptides allows understanding of forces involved in peptide assembly, as well as opens up a plethora of opportunities in regenerative medicine such as scaffolds for blood vessels, bone tissue engineering, and drug delivery (Khadka & Haynie, 2012).

In a typical electrospinning process, high voltage is applied to a polymeric solution forcing a droplet formation at the tip of a metallic needle and subsequent elongation leads to the formation of a Taylor cone. The high voltage provides the force to overcome the surface tension of the polymeric solution, and a resultant fiber jet is accelerated toward a grounded collector with the evaporation of solvent leading to the formation of solidified fibrous mesh at the collector (Baji, Mai, Wong, Abtahi, & Chen, 2010; Bhardwaj & Kundu, 2010; Frenot & Chronakis, 2003). Factors that influence the structure of the deposited fibers include solution parameters such as, conductivity of the solvents used, solution concentration, viscosity, and surface tension of the droplet, as well as the process parameters such as flow rate, distance between the capillary and collector, and applied voltage. Optimizing these parameters leads to the formation of continuous, bead-free nanofibers. On the other hand, environmental conditions such as percentage of relative humidity, temperature, and atmospheric pressure also play a significant role in the final morphology of the electrospun nanofibers (Haider, Haider, & Kang, 2018; Mendes et al., 2017). Optimal concentration of the polymeric solutions is required to induce chain entanglements, but extremely high concentrations can lead to highly viscous non-spinnable solutions. The main constraint with the use of short peptide sequences in the electrospinning process is the absence of "entanglements," which is essential for the formation of continuous electrospun fibers.

In this study, we have investigated the synthesis of biodegradable nanofibers composed of aromatic dipeptides using electrospinning conditions (Reches & Gazit, 2003; Singh et al., 2008). Aromatic amino acids such as tyrosine, and dityrosine crosslinks found in proteins such as resilin in cuticles of many insects and arthropods contribute to their mechanical stability due to high Young's modulus. Previous studies have shown that controlling the number of dityrosine crosslinks directly impacts the elastic modulus (Min et al., 2016; Partlow, Applegate, Omenetto, & Kaplan, 2016). Tyrosine-based dipeptides such as phenylalanine-tyrosine (FY), tryptophan-tyrosine (WY), and dityrosine (YY) were studied for their ability to form nanofibers under the influence of electrostatic forces. The presence of the aromatic groups and backbone interactions of the synthetic peptides used in this study enable strong interactions, promoting the formation of continuous, bead-free fibers. In this study, a combination of two electrophilic solvents with high vapor pressures, trifluoroacetic acid (TFA) and 1,1,1,3,3,3,-hexafluoroisopropanol (HFIP), were used to prepare the dipeptide solution at different concentrations (10–22% wt/vol). High concentrations of peptide solution (18% wt/vol) proved successful in the synthesis of nanofibers since these dimers lack the appropriate level of entanglements and a stable fiber jet could not be achieved at low concentrations due to lack of sufficient cohesive force between the molecules (Haider et al., 2018). The use of highly electrophilic solvents and high peptide concentrations were crucial factors required to obtain the viscosity necessary for the electrospinning of dipeptide-based nanofibers. Other parameters which could influence the final structure of the electrospun fibers, such as the needle to collector distance, applied voltage, flow rate, and relative humidity in the electrospinning chamber were modified (Table 1).

The influence of the various parameters on the morphology of the fibers was studied using scanning electron microscopy and conditions were modified to obtain continuous, bead-free nanofibers. The secondary structure of the synthesized fibers and influence of the electrostatic forces were analyzed using infrared spectroscopy, and Raman spectroscopy as well as circular dichroism (CD) techniques. Aromatic dipeptides demonstrate stable π-π stacking interactions due to the presence of a conjugated π-electron system and have the ability to self-assemble under suitable conditions. The IR peaks of the electrospun peptide fibers were compared with those of self-assembled peptide nanostructures to distinguish between secondary conformations and understand the influence of the synthesis process on the peptide secondary structures. Tyrosine-based materials are expected to have a high Young's modulus, therefore the loading moduli and the Young's moduli of the electrospun fibers were analyzed using nanoindentation.

One of the challenges in using electrospun protein or peptide fibers for biomedical applications is the lack of stability in aqueous environments and this lack of hydrolytic stability leads to the loss of fibrous morphology. To address this, we have chemically crosslinked the resultant nanofibers. Crosslinking increases the stability of the nanofibers in aqueous media through interconnecting the molecules and enhances their mechanical strength which influences the degradation rate of the protein-based electrospun nanofibers. Though the crosslinking process leads to structural stability, toxicity remains a concern and the degree of

TABLE 1 Electrospinning conditions used in the deposition of FY, WY, and YY dipeptides

Peptide	Flow rate (ml/hr)	Needle to collector distance (cm)	Voltage (kV)	Concentration (wt %)
FY	0.05	10–16	12–28	18% in 80:20 TFA: HFIP
WY	0.1	18–26	12–28	18% in 30:70 TFA: HFIP
YY	0.02	20	12–26	18% in 70:30 TFA:HFIP

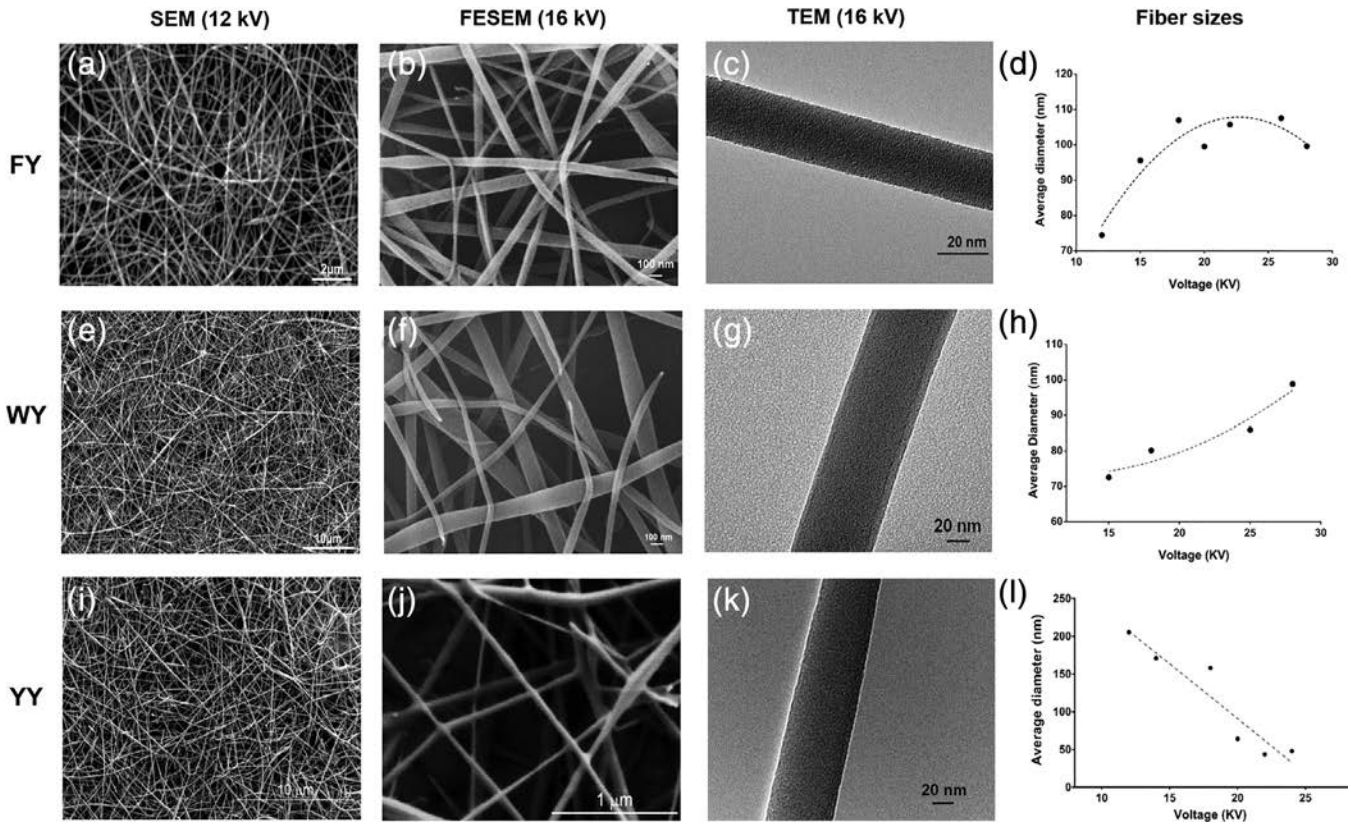

FIGURE 1 SEM micrographs of the electrospun FY, WY, and YY nanofibers (18% wt/vol solution) at different applied voltages. FY nanofibers synthesized with flow rate of 0.05 ml hr^{-1}, distance of 10 cm (a) 12 kV and (b) 16 kV; WY nanofibers synthesized with flow rate of 0.1 ml hr^{-1}, distance of 20 cm (e) 12 kV and (f) 16 kV; YY nanofibers synthesized with flow rate of 0.02 ml hr^{-1}, distance of 20 cm (i) 12 kV and (j) 16 kV; (c), (g), (k) TEM micrograph of the single nanofibers indicates smoothness of the nanofibers and absence of pores; (d), (h), (l) Analysis of influence of applied voltage on average nanofiber diameters measured using the SEM images in ImageJ

toxicity is dependent on the type of crosslinker used, the crosslinking mechanisms, and the conditions used for the process. Some crosslinkers that are typically used include genipin, glutaraldehyde (GA), N-(3-dimethylaminopropyl)-N-ethyl-carbodiimide hydrochloride (EDC), and EDC with N-hydroxy-sulfosuccinimide (EDC-NHS), hexamethylene-1, 6-diaminocarboxysulfonate (HDACS) and 1,6-diisohexanecyanate (HMDI) (Mendes et al., 2017; Nivison-Smith, Rnjak, & Weiss, 2010). However, some of the crosslinkers are toxic in nature and need to be eliminated completely before the fibers can be used for tissue engineering applications. Saturated GA vapor is commonly used to crosslink protein and carbohydrate-based fibers, however, it is toxic in nature (Lu, Sun, & Jiang, 2014; Mendes et al., 2017). GA produces heterogeneous crosslinks at the surface of the fibers via a reaction with the amine groups in the side-chains. HMDI is a bifunctional crosslinker which has recently been shown to improve the cytocompatibility and mechanical strength of the fibers (Delgado, Bayon, Pandit, & Zeugolis, 2015). In the case of HMDI, the highly reactive isocyanate groups were expected to crosslink the amine and hydroxyl groups in the peptide fibers. Initially, GA was used as the crosslinker, but HMDI in the vapor phase improved the stability of the peptide-based fibers in aqueous media. Nuclear magnetic resonance (NMR) spectroscopy was used to monitor the crosslinking efficiency since NMR is a widely used technique for characterization of crosslinking density at the molecular level. NMR presents advantages over other techniques such as equilibrium swelling due to its ease of use, rapid response time and the ability to analyze crosslinking density as well as distribution when specialized forms such as multiquantum NMR is used (Desai & Lee, 2015; Lai, Yu, & Tsai, 2016).

We have studied the biocompatibility of the peptide-based nanofibers as scaffolds for rat and human neural cell proliferation in vitro. PC12 cells were originally isolated from the rat adrenal pheochromocytoma and is a commonly used model for neural cell differentiation whereas SH-SY5Y is a human neuroblastoma cell line used as an in vitro model for dopaminergic neurons (Guroff, 1985; Xie, Hu, & Li, 2010). In this study, PC12 and SH-SY5Y cells were used to evaluate the biocompatibility of synthesized nanofibers and to understand their influence on cellular proliferation.

2 | MATERIALS AND METHODS

2.1 | Materials

Phenylalanine-tyrosine (FY), tryptophan-tyrosine (WY), and dityrosine (YY) peptides were purchased from Bachem. Trifluoroacetic acid

(TFA) and 1,1,1,3,3,3,-hexafluoroisopropanol (HFIP), glutaraldehyde (GA) and 1,6-diisohexanecyanate or hexamethylene diisocyanate (HMDI) were purchased from Sigma–Aldrich.

2.2 | Synthesis of nanofibers

A home-built electrospinning device with a syringe pump from Genie Touch Company, high voltage power supply from Gamma High Voltage Research Company, and an aluminum collector in horizontal configuration was used for the deposition of nanofibers. A 25-gauge needle was used for the fiber deposition. The collector was fixed and grounded. The dipeptides were dissolved in an appropriate solvent to make 18–20% wt/vol solutions prior to mixing using a vortexer. All the experiments were performed at room temperature and ambient atmospheric conditions (relative humidity below 25%). The nanofibers were collected on various substrates: aluminum foil, silicon wafers, glass coverslips, and conductive tape to obtain freestanding fiber sheets.

2.3 | Crosslinking experiments

One set of electrospun fibers were exposed to glutaraldehyde (25 μL GA) vapors (25%) for 24 hr to achieve crosslinking and improve stability of the fibers in aqueous solutions (Lu et al., 2014). Another set of the fibers were exposed to vapors of 1,6-diisohexanecyanate (35 μL of HMDI) for 48 hr to be crosslinked (Nivison-Smith et al., 2010). The fibers were then stored under vacuum for 24–48 hr to eliminate excess solvent vapors. All the fibers used for cell culture were washed with water twice and soaked in water overnight to eliminate any residual solvents used in the synthesis process and excess crosslinking agents.

2.4 | Morphological characterization

The morphology of the deposited nanofibers were observed using the JEOL JSM 5610 SEM, Hitachi SU5000 and the JEOL JSM 7401F field-emission SEM at varying accelerating voltages of 5–20 kV. The samples were sputter coated with a thin layer of gold before observation. For the transmission electron microscopy, the fibers were deposited on 400-mesh copper grids with carbon films from Ted Pella before imaging in the Phillips EM400T TEM. The dimensions of the nanofibers were measured using the ImageJ software.

2.5 | FTIR and Raman spectroscopy

Infrared (IR) spectra were obtained using the Digilab Excalibur FTS3000MX and the win-IR Pro program at a 2 cm^{-1} resolution. The deposited peptide fibers were ground with IR grade potassium bromide (KBr) at a ratio of 1:20 and pressed into a pellet for the spectral measurement. A custom-built confocal μRaman setup from Witec Instruments, with a spectrometer (1800/mm grating) of high spatial resolution down to 1 cm^{-1} was used in this study. The excitation source was a 75 mW, 532 nm diode pumped solid-state laser.

2.6 | NMR

Two milligrams of the uncrosslinked electrospun FY nanofibers and crosslinked with HMDI were dissolved in deuterated DMSO and a Bruker AVANCE III HD 400 MHz High-Performance Digital NMR was used to obtain their 1H spectra. The chemical shifts were analyzed using MestReNova package.

2.7 | CD spectroscopy (CD)

The CD analysis of the FY, WY, and YY nanofibers was performed on a Jasco J720 spectropolarimeter averaged over three scans with a 190–300 nm range, and 100 nm/min speed. The CD data from nanofiber solutions of concentrations 0.01 mg/ml was processed using CDSSTR, CONTIN-LL, and SELCON3 methods available on Dichroweb. Stock solutions of the nanofibers were diluted in double distilled water to final concentrations of 0.01 mg/ml.

2.8 | Atomic force microscopy (AFM)

A Park Systems 100-XE Atomic Force Microscope was used in the noncontact mode to capture topography of the peptide nanofibers. Non-contact mode cantilevers of spring constant of 25–40 N/m were used to obtain high-resolution images.

2.9 | Nanoindentation

Agilent Nanoindenter XP MTS instrument with a continuous stiffness measurement (CSM) option was used to obtain the bulk loading modulus and Young's modulus of the peptide fibers on a silicon substrate. Contact force was measured with a cylindrical flat-punch indenter.

2.10 | Cell culture

Rat pheochromocytoma cells (PC12) and human neuroblastoma cells (SH-SY5Y) from the American Type Culture Collection (ATCC) were cultured at 37°C, 95% humidity, and 5% CO_2. The PC12 cells were maintained in RPMI 1640 supplemented with 10% heat-inactivated horse serum and 5% fetal bovine serum (FBS) (Greene & Tischler, 1976). Similarly, SH-SY5Y cells were maintained in 1:1 F-12, EMEM supplemented with 5% FBS. FY nanofibers were deposited on glass coverslips (5 mm diameter) treated with aminosilane (5% in methanol) for cell culture testing. PC12 cells were seeded on the coverslips with

nanofibers (5×10^3 cells/coverslip) and the cell viability was recorded on days 3, 5, and 7 using the 3-(4,5-dimethylthiazol-2-yl)-2,5-diphenyltetrazolium bromide (MTT) reagent at a final concentration of 0.5 mg/ml (Gerlier & Thomasset, 1986). Absorbance at 570 nm was measured using a Multiskan™ FC microplate reader (Thermo Scientific™). Confocal images of SH-SY5Y and PC12 cells cultured on nanofibers were obtained after the cells were fixed on third day using 2.5% glutaraldehyde. The cells were stained with phalloidin rhodamine and nuclear stain DAPI before they were imaged using a confocal microscope Zeiss 710 (Carl Zeiss, Thornwood, NY). SEM images were also obtained for the fixed cells grown on the nanofibers following subsequent fixing in 1% osmium tetroxide, washing with phosphate-buffered saline (PBS). The samples were dehydrated and finally dried using a chemical alternate to critical point drying, which utilizes hexamethyldisilazane (HMDS).

3 | RESULTS

Continuous, bead-free nanofibers were obtained using optimum spinning conditions for the FY peptide and are shown in Figure 1a (flow rate of 0.05 ml/hr, collector-needle of 10 cm, and voltage of 12 kV). Based on the SEM observations, the factors that influenced the FY nanofibers synthesis and structure were high peptide concentration (18% wt/vol) and the voltages used. The use of voltages in the range of 12–20 kV during the synthesis of the FY nanofibers indicate that lower applied voltages favor the formation of bead-free nanofibers (Figure 1S In SI, Figure 1a–c) and 12 kV was found to be the nominal voltage to obtain individual nanofibers. Synthesis of smooth nanofibers and disappearance of beads at lower voltages is in agreement with previous studies on the electrospinning of polymers (Buchko, Kozloff, & Martin, 2001; Deitzel, Kleinmeyer, Harris, & Beck Tan, 2001; Demir, Yilgor, Yilgor, & Erman, 2002; Haider et al., 2018). The diameter of FY nanofibers measured using the ImageJ software indicates a diameter range of 95 to 107 nm with the average diameter being ~98 nm, as confirmed by the FESEM imaging (Figure 1c). The established optimal parameters were used to deposit free-standing films of the FY nanofibers (Figure 2S in SI). Similar deposition conditions were initially utilized for the deposition of WY dipeptide, however, continuous nanofibers were obtained at a larger needle-collector distances (20 cm). For the WY dimer, the influence of the voltage on the morphology of the nanofibers was also evident. Decreasing the voltage from 25 to 12 kV reduced the appearance of beads in the nanofibers (Figure 1a,e,i).

Nominal increase in the diameter with an increase in the applied voltage was also observed in the nanofibers composed both the FY and WY peptides. Similar effects were observed in prior studies involving poly (vinyl alcohol) and polyethylene oxide (Deitzel et al., 2001; Zhang, Yuan, Wu, Han, & Sheng, 2005). But in the case of the YY nanofibers (Figure 1l), the nanofiber diameters reduced with the increasing applied voltage and remained constant in the higher voltage range during the deposition process. Though the fibers were ultra-thin, beads appeared in the YY fibers at voltages higher than 20 kV. This is in agreement with prior studies, which have shown that the shape of the originating jet is dependent on the voltage and this leads to an increased appearance of beads or other defects such as fragmented fibers as observed in the 24 kV deposition (Figure 1S in SI). The TEM micrographs of the dipeptide fibers show the structure of individual fibers and confirm the smoothness of the fibers deposited at 16 kV (Figure 1c,g,k). Individual nanofibers appeared to have uniform diameter and were cylindrical in shape and such cylindrical nanofibers are suitable for biological applications.

The peptide nanofibrous mats exhibit stiffness (loading moduli) in the range of 0.5–4 GPa, as tested using the nanoindenter XP. Figure 3c shows the representative load–displacement curve of electrospun FY nanofibers. Even though the YY nanofibers were found to have the lowest stiffness (0.5 GPa) in all the tested electrospun nanofibers, the stiffness is high compared to other electrospun biodegradable polymeric fibers (Baker, Banerjee, Bonin, & Guthold, 2016). The variations observed in the stiffness observed could be attributed to the differences in the peptide composition, nanofiber diameter, as well as porosity. It is important to note there can be deformation of fibers around the indenter and it is difficult to accurately estimate the contact area during the indentation of nanofibrous surface Therefore, the results are indicative of general trends in the stiffness and is in close agreement with self-assembled aromatic peptide-based nanomaterials (Adler-Abramovich et al., 2006).

In order to analyze the chemical characteristics of the nanofibers, FTIR, and Raman spectroscopy were performed. The deconvoluted FTIR spectra of the secondary structure region of the nanofibers as shown in Figure 2a–c, indicate that the changes in the chemical structure can be attributed to the slight denaturation of peptides in solvents used. The influence of the solvents on the peptide structure was monitored using FTIR spectra (Figure 3S(a) of SI). Due to solvent interactions, some of the FY peaks have disappeared due to partial decomposition. Reduction and complete elimination of TFA for fabrication of nanofibers is a future research direction. The prominent C—O and C—N bond peaks at 1100 cm^{-1} and 1200 cm^{-1}, and 1670 cm^{-1} for C⍰C were observed both in the FY and WY nanofibers and the small peak shift in the nanofibers is related to conjugation which results in decreased wavenumbers (see Figure 2a,b, inset). The 1600 cm^{-1} peak related to the aromatic ring structure was not observed in some of the fiber samples which was attributed to the effect of the solvent used, TFA. The peaks around 1680 cm^{-1} attributed to the C⍰C and C⍰O bonds, indicate the preservation of the structure in the nanofibers after exposure to the electrostatic force. The secondary structure of the electrospun samples were compared with self-assembled peptides in solution to understand the differences in behavior and results were tabulated (Table S1). The main contribution to the secondary structure of the dipeptide nanofibers was equally distributed between β-sheets and β-turns whereas the self-assembled structures had a highest contribution from the β-turns. The analyses indicated that the solvents used influenced the chemical properties of the peptides due to slight denaturation but the electrostatic forces themselves do not significantly influence the chemical structures of the peptides. FTIR spectra of the crosslinked FY, WY, YY

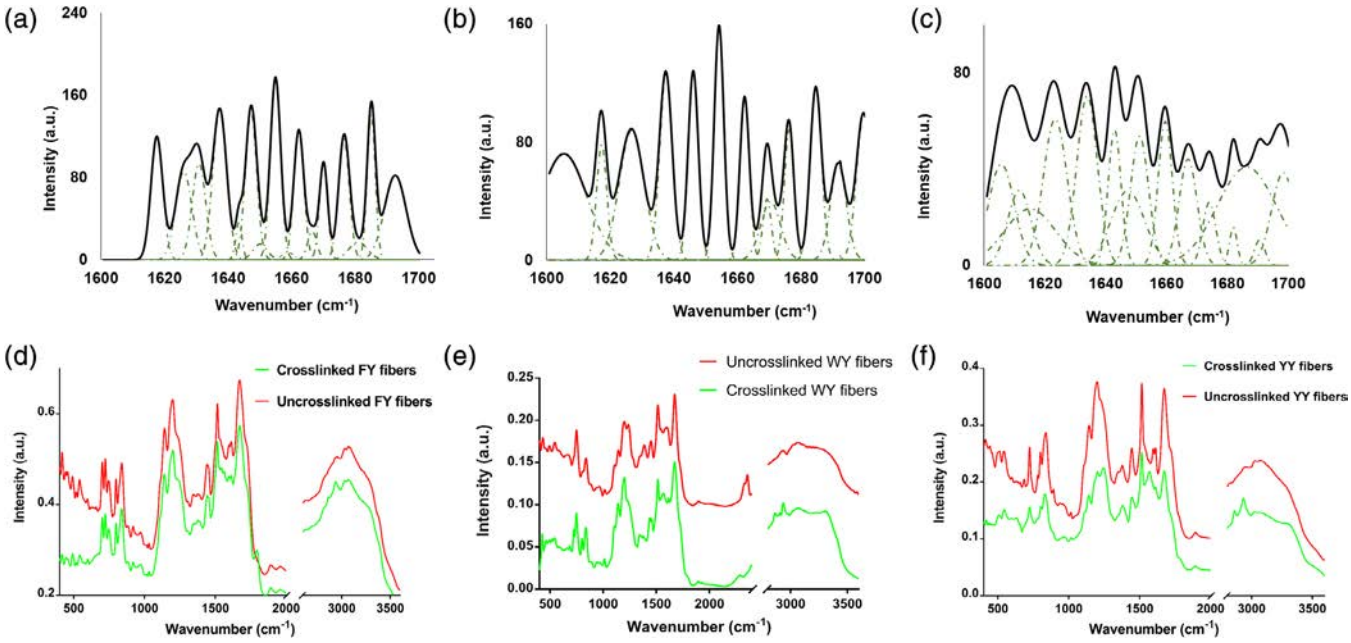

FIGURE 2 Deconvoluted FTIR spectra of secondary structure in the amide I region. (a) FY nanofibers; (b) WY nanofibers; (c) YY nanofibers; comparison of the FTIR of uncrosslinked and crosslinked fibers. (d) FY nanofibers; (e) WY nanofibers; and (f) YY nanofibers

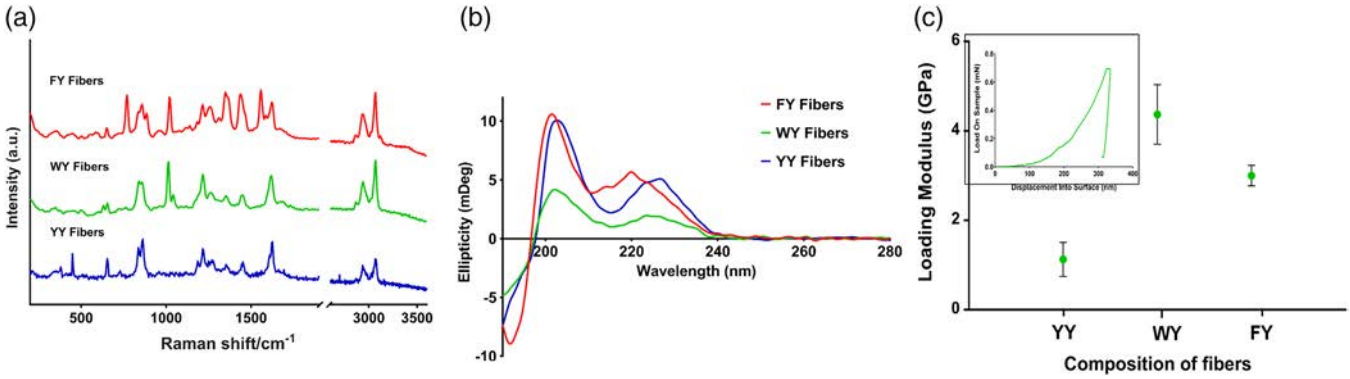

FIGURE 3 (a) Raman analysis of FY nanofibers, WY nanofibers and YY nanofibers; (b) representative nanoindentation curve of FY nanofibers and loading moduli of the nanofibers; (d) CD spectral analysis of FY, WY, and YY nanofibers

nanofibers are shown in Figure 2d–f, respectively. The peak at 1788 cm^{-1} is a carbonyl peak attributed to the crosslinker HMDI. The Amide I region identical Amide II peak intensities in the 1530 cm^{-1} region indicated. A prominent peak appears at 2954 cm^{-1} indicative of C—H bonding in the crosslinked fibers. Based on these observations, we can conclude that crosslinking using HMDI did not significantly alter the secondary structures of the fibers.

Raman analysis of the electrospun nanofibers also confirmed the contribution of the dominant β-sheet secondary structure in the deposited nanofibers (Figure 3a). Benzene ring deformation, ring breathing and stretching modes at ~640 cm^{-1}, ~840 cm^{-1} and ~1015 cm^{-1}, respectively were undisturbed due to the C—C bonds of the dipeptide units (Tsuboi et al., 1998). The amide III region (1230–1340 cm^{-1}), plays a significant role in the secondary structure along with the Amide I region (Rygula et al., 2013). N—H bending, N—C stretching and skeletal stretches in the ~1229–1235 cm^{-1} region indicate the presence of β-sheet and turns conformations (Figure 3a) (Chi, Chen, Holtz, & Asher, 1998). The peaks at ~1365 cm^{-1} and 1455 cm^{-1} are attributed to the C_α—H bending, CH_2 wagging and scissoring. The shift observed in the C_α—H bending peaks toward lower frequencies (from ~1390 cm^{-1}) is attributed to the decrease in α-helical content and is indicative of the formation of higher order β-sheet and turns. Amide II peaks (~1550 cm^{-1}) usually attributed to N—H bending and N—C stretching, unlike in the FTIR readings, were negligible. The carbonyl peak (C⍰O) along with N—H deformation stretching and C—N stretching were observed in the Amide-I region (1625–1730 cm^{-1}) for the oligopeptide monomers but the electrospun nanofibers have peaks in a lower frequency region (1613–1680 cm^{-1}). This could be due to the conjugation and weak antiparallel β-sheets and β-turns interaction. Typically, a broad secondary structure region (1645–1680 cm^{-1}) indicates the presence of α-helix, β-sheet and turns but the broad band was centered at ~1670 cm^{-1} in the electrospun samples due to the dominant β-sheet

structure (Tarhan, Tarhan, & Harsa, 2014). The N—H stretch at ~3200–3300 cm^{-1} were observed in double bands, indicating the presence of a primary amine. The FTIR and Raman data indicate that the secondary structural arrangements found in the nanofibers were predominantly β-sheets and β-turns in nature (Sereda, Ralbovsky, Vasudev, Naik, & Lednev, 2016; Tarhan et al., 2014; Zhu, Isaacs, Hecht, & Barron, 2005). Raman analysis of the crosslinked fibers indicate no major peak shifts in the secondary structural region except for the prominent carbonyl peak (Figure 4S in SI).

The peak positions in the secondary FTIR spectra of the electrospun nanofibers differed significantly from the peaks observed in the self-assembled structures leading to the conclusion that the process of electrospinning is one of forced assembly and not self-assembly. In addition to the secondary structural analysis, the CD spectra of WY, YY, and FY electrospun nanofibers was also obtained as shown in Figure 3b. Comparison between the experimental data from CD spectroscopy and theoretical data from Dichroweb showed the predominant secondary structures present in the electrospun nanofibers. The predominant secondary structural arrangement observed in both the WY and YY nanofibers were β-strands. The peaks around 200 and 220 nm, in WY and YY nanofibers corresponded to the n-π* and π-π* transitions, indicating the presence of β-strands. FY nanofibers however had a combination of both α-helices and β-strands as secondary structures. CD spectral analysis of the electrospun fibers crosslinked using HMDI do not indicate any changes in ellipticity (Figure 4S(b) in SI).

One of the concerns with electrospun proteins and peptides is their stability in physiological conditions. Initially, crosslinking using two performed using two crosslinkers, GA and HMDI to improve the stability of the peptide nanofibers in aqueous solutions (Figure 5S in SI and Figure 4a & b, respectively) however due to the observed swelling in the individual nanofibers in the case of GA as the crosslinker subsequent sample crosslinking was performed using HMDI. AFM images obtained after the HMDI-crosslinked nanofibers were soaked in a buffer solution for a week also indicate that the fibrous surface topography was intact following the crosslinking using HMDI and the measured diameters also indicate no swelling after being immersed in a buffer for 7 days (Figure 4a). NMR analysis of the synthesized uncrosslinked and crosslinked nanofibers in presence of HMDI indicate extra chemical shifts in the spectra of crosslinked nanofibers (Figure 4c, d). The number of protons in the crosslinked nanofibers has significantly increased in comparison to the uncrosslinked nanofibers, due to the crosslinking of the dimers. The additional peaks in 0–4 and 6–7 regions of the H-NMR spectra correspond to the aliphatic and NH protons of the HMDI crosslinker (OCN—C—$[CH_2]_4$—C—NCO).

The cytotoxicity concerns with the use of crosslinkers such as HMDI were addressed using MTT assay for the pheochromocytoma, PC12 cell viability on the nanofiber surface. The MTT average

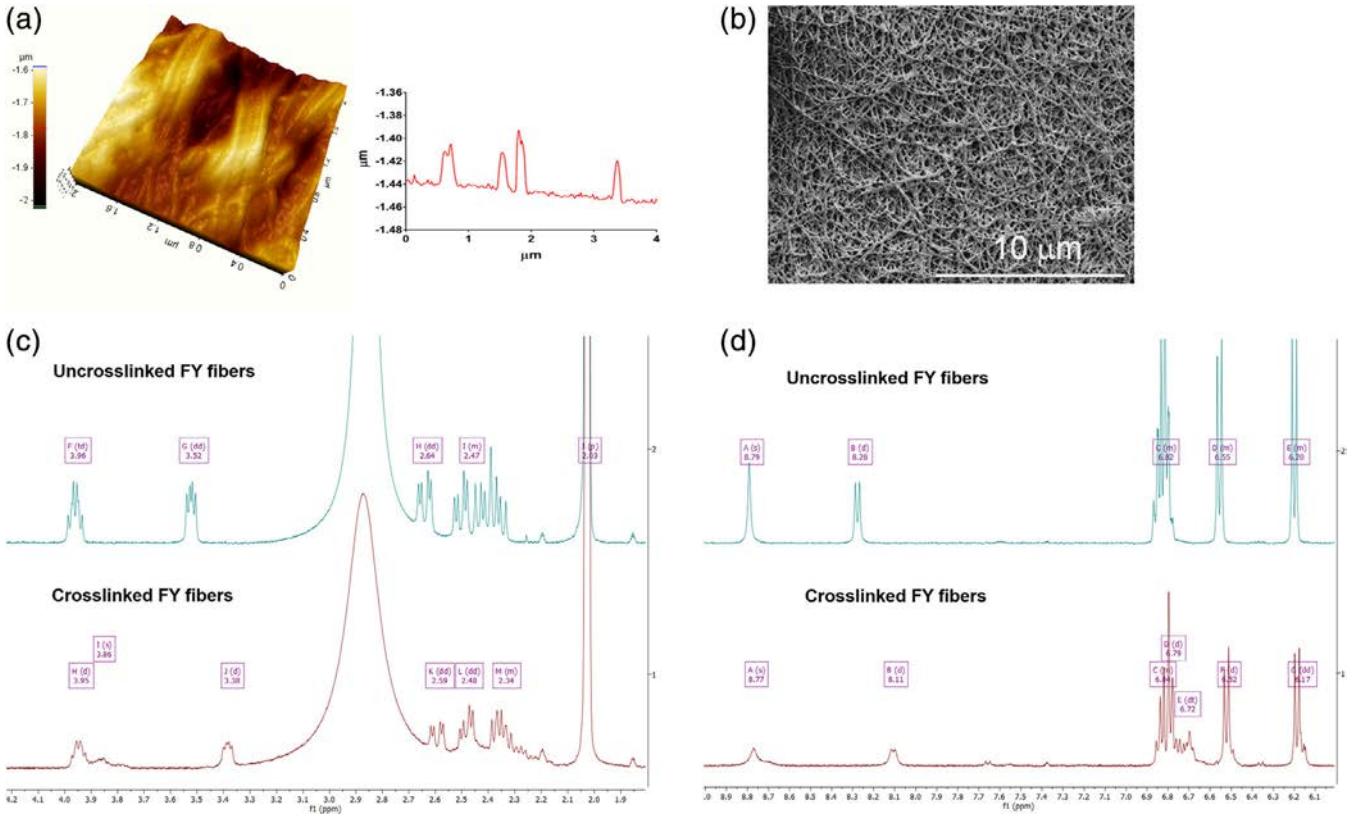

FIGURE 4 (a–c) 3D AFM topography of crosslinked FY nanofibers on a glass coverslip; SEM micrographs of the FY nanofibers after exposure to HMDI (10%) vapors overnight after exposure to water for 24 hr with no observed swelling or changes in morphology; (c) and (d) NMR analysis of the uncrosslinked FY nanofibers and following crosslinking with HMDI (10%)

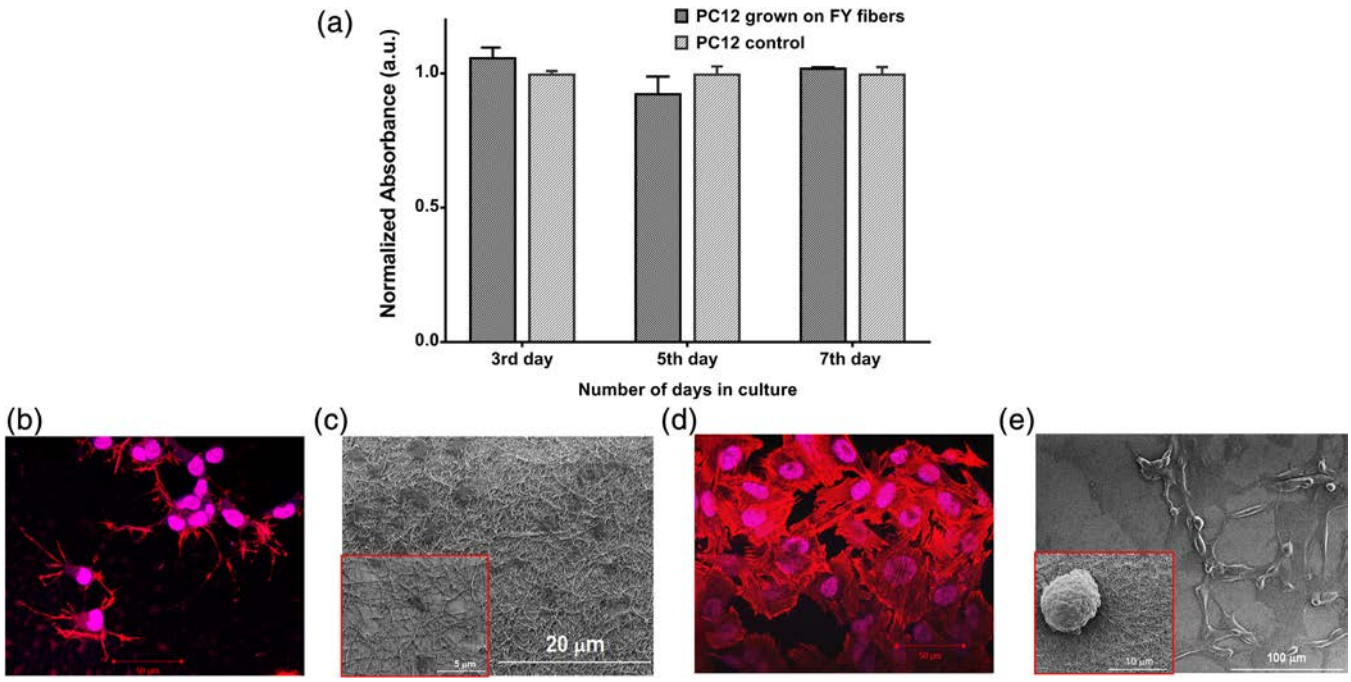

FIGURE 5 (a) Normalized absorbance intensities of the MTT assay of PC12 cells on FY nanofibers on days 3, 5, and day 7. Confocal micrographs of (b) SH-SY5Y cells with neurite projections, (d) PC12 cells on FY nanofibers and SEM images of (c) SH-SY5Y, (e) PC12 cells on FY fibers on third day

absorbance for the crosslinked nanofibers was compared to a control (glass coverslip). Figure 5a shows an overall increase in cell count and activity was observed as the days progressed from 1 to 7 days in the case of FY fibers, which was similar to WY and YY fibers (Figure 7S of SI). There was a slight drop in the activity of the cells in the control between day 5 and 7. This drop could be attributed to the increase in confluency of the cells at day 7. Though the absorbance values of the cells grown on nanofibers was slightly different than the absorbance of the control, no significant activity difference with a *p*-value of 0.9328 (paired *t* test) was observed indicating that the crosslinked nanofibers were not cytotoxic to the PC12 cells. Additionally, the PC12 cells were stained for the live/dead assay to evaluate cell viability (Figure 6S in SI).

The rat pheochromocytoma cells (PC12) and human neuroblastoma cells (SH-SY5Y) grown and fixed on crosslinked FY nanofibers after 72 hr of seeding were stained with phalloidin rhodamine and nuclear stain DAPI before they were imaged using confocal microscopy, as shown in Figure 5b,c. SEM images of the PC12 and the SH-SY5Y cells fixed at 72 hr after seeding in the confirm the attachment of the cells on FY electrospun nanofibers and cellular proliferation as shown Figure 5 d,e. The cells demonstrated elliptical morphologies with multiple contacts with nanofibers and neurite projections. Depending on future studies, such electrospun nanofiber scaffolds could be potentially useful as neural cell regeneration scaffolds.

4 | DISCUSSION

Electrospinning as a synthesis process is rapid, efficient, and can be used to control the chemical composition and material properties of engineered materials. The ability to successfully produce nanofibers from oligomeric peptides indicates the role of strong intermolecular forces such as hydrogen bonding and π-π-stacking along with the increased Coulombic forces and surface tension due to the applied electrostatic field. This study further characterizes the influence of peptide concentration, input voltages, distances, and flow rates, which affect the electrospinning of aromatic dipeptides. Each of these parameters impacts the formation and morphology of the nanofibers formed during the electrospinning process. The identification of suitable electrospinning solvents for the peptides studied (a combination of TFA/HFIP) has opened a design space where peptides of varying compositions can be tested for their ability to form stable nanofibers. The solvents used may promote the formation of secondary structures observed in the electrospun peptides such as β-sheets in proteins/peptides with a primary sequence that favors this conformational arrangement.

The comparison of the secondary structures of the electrospun samples using FTIR indicates that the structures are different from the ones in the self-assembled structures. The conjugated π-electron system in aromatic dipeptides allows self-assembly under suitable conditions. Even though the fibers demonstrated stable π-π interactions, the IR peaks in the Amide I region (secondary structure) were found to be significantly different leading to the conclusion that the process of electrospinning is one of forced assembly and not self-assembly (Table 1S in SI). Cytotoxicity was not observed in the neuronal cells cultured on the crosslinked nanofibers and the composition of the nanofibers with tryptophan and tyrosine, both of which have high redox potential and support long range electron transfer implies that future cellular testing can include electrical stimulation of the neuronal cells (Warren, Winkler, & Gray, 2012). Such electrospun peptide

nanofibers hold promise in regenerative medicine and biomedical engineering applications such as scaffolds for tissue engineering, tissue repair, and sutures. Furthermore, electrospun peptide coatings can potentially enhance the integration of implants by enabling functional coatings through the replacement of conventional polymer coatings with bioactive peptide coatings (Pugliese & Gelain, 2017; Tayi et al., 2014). The utilization of conventional polymers in biomedical applications could be reduced in the future, as a result of the ability to tailor the sequence of amino acids for such specific applications.

ACKNOWLEDGMENTS

The electron microscopy images in this work were obtained using a scanning electron microscope supported by the National Science Foundation under Grant No. 1726239. We acknowledge the support by the University of Massachusetts Dartmouth Provost's office for the multidisciplinary seed funding, and faculty start-up grants. We are grateful to the Materials and Manufacturing directorate of the Air Force Research Laboratory for allowing us access to their CD spectrometer and the nanoindenter XP for materials characterization. We thank Anver Basha Shaik of the National Institute of Drug Abuse for his assistance in the analysis of NMR data.

CONFLICT OF INTEREST

The authors have no conflict of interests to declare.

AUTHOR CONTRIBUTIONS

The manuscript was written through contributions of all authors. All authors have given approval to the final version of the manuscript.

ORCID

Milana C. Vasudev https://orcid.org/0000-0003-0766-1103

REFERENCES

Adler-Abramovich, L., Aronov, D., Beker, P., Yevnin, M., Stempler, S., Buzhansky, L., … Gazit, E. (2009). Self-assembled arrays of peptide nanotubes by vapour deposition. *Nature Nanotechnology*, *4*(12), 849–854.

Adler-Abramovich, L., Reches, M., Sedman, V. L., Allen, S., Tendler, S. J., & Gazit, E. (2006). Thermal and chemical stability of diphenylalanine peptide nanotubes: Implications for nanotechnological applications. *Langmuir*, *22*(3), 1313–1320.

Baji, A., Mai, Y.-W., Wong, S.-C., Abtahi, M., & Chen, P. (2010). Electrospinning of polymer nanofibers: Effects on oriented morphology, structures and tensile properties. *Composites Science and Technology*, *70*(5), 703–718.

Baker, S. R., Banerjee, S., Bonin, K., & Guthold, M. (2016). Determining the mechanical properties of electrospun poly-ε-caprolactone (PCL) nanofibers using AFM and a novel fiber anchoring technique. *Materials Science and Engineering: C*, *59*, 203–212.

Bhardwaj, N., & Kundu, S. C. (2010). Electrospinning: A fascinating fiber fabrication technique. *Biotechnology Advances*, *28*(3), 325–347.

Buchko, C. J., Kozloff, K. M., & Martin, D. C. (2001). Surface characterization of porous, biocompatible protein polymer thin films. *Biomaterials*, *22*(11), 1289–1300.

Chi, Z., Chen, X., Holtz, J. S., & Asher, S. A. (1998). UV resonance Raman-selective amide vibrational enhancement: Quantitative methodology for determining protein secondary structure. *Biochemistry*, *37*(9), 2854–2864.

Deitzel, J. M., Kleinmeyer, J., Harris, D., & Beck Tan, N. C. (2001). The effect of processing variables on the morphology of electrospun nanofibers and textiles. *Polymer*, *42*(1), 261–272.

Delgado, L. M., Bayon, Y., Pandit, A., & Zeugolis, D. I. (2015). To cross-link or not to cross-link? Cross-linking associated foreign body response of collagen-based devices. *Tissue Engineering. Part B, Reviews*, *21*(3), 298–313.

Demir, M. M., Yilgor, I., Yilgor, E., & Erman, B. (2002). Electrospinning of polyurethane fibers. *Polymer*, *43*(11), 3303–3309.

Desai, M. S., & Lee, S.-W. (2015). Protein-based functional nanomaterial design for bioengineering applications. *WIREs Nanomedicine and Nanobiotechnology*, *7*(1), 69–97.

Elsabee, M. Z., Naguib, H. F., & Morsi, R. E. (2012). Chitosan based nanofibers, review. *Materials Science and Engineering: C*, *32*(7), 1711–1726.

Frenot, A., & Chronakis, I. S. (2003). Polymer nanofibers assembled by electrospinning. *Current Opinion in Colloid & Interface Science*, *8*(1), 64–75.

Gerlier, D., & Thomasset, N. (1986). Use of MTT colorimetric assay to measure cell activation. *Journal of Immunological Methods*, *94*(1–2), 57–63.

Grafahrend, D., Heffels, K.-H., Beer, M. V., Gasteier, P., Möller, M., Boehm, G., … Groll, J. (2010). Degradable polyester scaffolds with controlled surface chemistry combining minimal protein adsorption with specific bioactivation. *Nature Materials*, *10*, 67.

Greene, L. A., & Tischler, A. S. (1976). Establishment of a noradrenergic clonal line of rat adrenal pheochromocytoma cells which respond to nerve growth factor. *Proceedings of the National Academy of Sciences*, *73*(7), 2424–2428.

Guroff, G. (1985). PC12 cells as a model of neuronal differentiation. In J. E. Bottenstein & G. Sato (Eds.), *Cell culture in the neurosciences* (pp. 245–272). Boston, MA: Springer US.

Habibi, N., Kamaly, N., Memic, A., & Shafiee, H. (2016). Self-assembled peptide-based nanostructures: Smart nanomaterials toward targeted drug delivery. *Nano Today*, *11*(1), 41–60.

Haider, A., Haider, S., & Kang, I.-K. (2018). A comprehensive review summarizing the effect of electrospinning parameters and potential applications of nanofibers in biomedical and biotechnology. *Arabian Journal of Chemistry*, *11*(8), 1165–1188.

Holzapfel, B. M., Reichert, J. C., Schantz, J.-T., Gbureck, U., Rackwitz, L., Nöth, U., … Hutmacher, D. W. (2013). How smart do biomaterials need to be? A translational science and clinical point of view. *Advanced Drug Delivery Reviews*, *65*(4), 581–603.

Kai, D., Liow, S. S., & Loh, X. J. (2014). Biodegradable polymers for electrospinning: Towards biomedical applications. *Materials Science and Engineering: C*, *45*, 659–670.

Khadka, D. B., & Haynie, D. T. (2012). Protein- and peptide-based electrospun nanofibers in medical biomaterials. *Nanomedicine: Nanotechnology, Biology and Medicine*, *8*(8), 1242–1262.

Koh, H. S., Yong, T., Chan, C. K., & Ramakrishna, S. (2008). Enhancement of neurite outgrowth using nano-structured scaffolds coupled with laminin. *Biomaterials*, *29*(26), 3574–3582.

Lai, T. C., Yu, J., & Tsai, W. B. (2016). Gelatin methacrylate/carboxybetaine methacrylate hydrogels with tunable crosslinking for controlled drug release. *Journal of Materials Chemistry B*, *4*(13), 2304–2313.

Lu, W., Sun, J., & Jiang, X. (2014). Recent advances in electrospinning technology and biomedical applications of electrospun fibers. *Journal of Materials Chemistry B*, *2*(17), 2369–2380.

Mendes, A. C., Stephansen, K., & Chronakis, I. S. (2017). Electrospinning of food proteins and polysaccharides. *Food Hydrocolloids*, *68*, 53–68.

Min, B.-M., Lee, G., Kim, S. H., Nam, Y. S., Lee, T. S., & Park, W. H. (2004). Electrospinning of silk fibroin nanofibers and its effect on the adhesion

and spreading of normal human keratinocytes and fibroblasts in vitro. *Biomaterials*, *25*(7–8), 1289–1297.

Min, K.-I., Yun, G., Jang, Y., Kim, K.-R., Ko, Y. H., Jang, H.-S., … Kim, D.-P. (2016). Covalent self-assembly and one-step photocrosslinking of tyrosine-rich oligopeptides to form diverse nanostructures. *Angewandte Chemie International Edition*, *55*(24), 6925–6928.

Nivison-Smith, L., Rnjak, J., & Weiss, A. S. (2010). Synthetic human elastin microfibers: Stable cross-linked tropoelastin and cell interactive constructs for tissue engineering applications. *Acta Biomaterialia*, *6*(2), 354–359.

Nuansing, W., Frauchiger, D., Huth, F., Rebollo, A., Hillenbrand, R., & Bittner, A. M. (2013). Electrospinning of peptide and protein fibres: Approaching the molecular scale. *Faraday Discussions*, *166*, 209–221.

Partlow, B. P., Applegate, M. B., Omenetto, F. G., & Kaplan, D. L. (2016). Dityrosine cross-linking in designing biomaterials. *ACS Biomaterials Science & Engineering*, *2*(12), 2108–2121.

Pugliese, R., & Gelain, F. (2017). Peptidic biomaterials: From self-assembling to regenerative medicine. *Trends in Biotechnology*, *35*(2), 145–158.

Reches, M., & Gazit, E. (2003). Casting metal nanowires within discrete self-assembled peptide nanotubes. *Science*, *300*(5619), 625–627.

Rho, K. S., Jeong, L., Lee, G., Seo, B.-M., Park, Y. J., Hong, S.-D., … Min, B.-M. (2006). Electrospinning of collagen nanofibers: Effects on the behavior of normal human keratinocytes and early-stage wound healing. *Biomaterials*, *27*(8), 1452–1461.

Rygula, A., Majzner, K., Marzec, K. M., Kaczor, A., Pilarczyk, M., & Baranska, M. (2013). Raman spectroscopy of proteins: A review. *Journal of Raman Spectroscopy*, *44*(8), 1061–1076.

Sereda, V., Ralbovsky, N. M., Vasudev, M. C., Naik, R. R., & Lednev, I. K. (2016). Polarized raman spectroscopy for determining the orientation of di-d-phenylalanine molecules in a nanotube. *Journal of Raman Spectroscopy*, *47*(9), 1056–1062.

Singh, G., Bittner, A. M., Loscher, S., Malinowski, N., & Kern, K. (2008). Electrospinning of diphenylalanine nanotubes. *Advanced Materials*, *20*(12), 2332–2336.

Tarhan, Ö., Tarhan, E., & Harsa, Ş. (2014). Investigation of the structure of alpha-lactalbumin protein nanotubes using optical spectroscopy. *Journal of Dairy Research*, *81*(1), 98–106.

Tayi, A. S., Pashuck, E. T., Newcomb, C. J., McClendon, M. T., & Stupp, S. I. (2014). Electrospinning bioactive supramolecular polymers from water. *Biomacromolecules*, *15*(4), 1323–1327.

Tsuboi, M., Ezaki, Y., Aida, M., Suzuki, M., Yimit, A., Ushizawa, K., & Ueda, T. (1998). Raman scattering tensors of tyrosine. *Biospectroscopy*, *4*(1), 61–71.

Vasudev, M. C., Koerner, H., Singh, K. M., Partlow, B. P., Kaplan, D. L., Gazit, E., … Naik, R. R. (2014). Vertically aligned peptide nanostructures using plasma-enhanced chemical vapor deposition. *Biomacromolecules*, *15*(2), 533–540.

Warren, J. J., Winkler, J. R., & Gray, H. B. (2012). Redox properties of tyrosine and related molecules. *FEBS Letters*, *586*(5), 596–602.

Wu, C.-S. (2014). Mechanical properties, biocompatibility, and biodegradation of cross-linked cellulose acetate-reinforced polyester composites. *Carbohydrate Polymers*, *105*, 41–48.

Xie, H.-R., Hu, L.-S., & Li, G.-Y. (2010). SH-SY5Y human neuroblastoma cell line: In vitrocell model of dopaminergic neurons in Parkinson's disease. *Chinese Medical Journal*, *123*(8), 1086–1092.

Zhang, C., Yuan, X., Wu, L., Han, Y., & Sheng, J. (2005). Study on morphology of electrospun poly(vinyl alcohol) mats. *European Polymer Journal*, *41*(3), 423–432.

Zhang, H., Fei, J., Yan, X., Wang, A., & Li, J. (2015). Enzyme-responsive release of doxorubicin from monodisperse dipeptide-based nanocarriers for highly efficient cancer treatment in vitro. *Advanced Functional Materials*, *25*(8), 1193–1204.

Zhu, F., Isaacs, N. W., Hecht, L., & Barron, L. D. (2005). Raman optical activity: A tool for protein structure analysis. *Structure*, *13*(10), 1409–1419.

SUPPORTING INFORMATION

Additional supporting information may be found online in the Supporting Information section at the end of this article.

How to cite this article: Hamedani Y, Macha P, Evangelista EL, et al. Electrospinning of tyrosine-based oligopeptides: Self-assembly or forced assembly? *J Biomed Mater Res*. 2020;108: 829–838. https://doi.org/10.1002/jbm.a.36861